A Liquid-Metal Wearable Sensor for Respiration Monitoring: Biomechanical Requirements, Modeling, Design, and Characterization

Fabio Lazzari, Marco Gaviati, Lorenzo Garavaglia, Jacopo Romanò, and Simone Pittaccio

***Abstract*—Liquid metals are metals in the liquid state at room temperature; they mostly belong to the alloys of Ga and In. These alloys have attracted attention because of their capacity to conduct electricity and heat, coupled with unique mechanical properties, which allow them to undergo extreme deformations, and self-heal. Their many possible applications range from microfluidics to soft robotics. They are particularly interesting for the fabrication of wearable sensing devices. We design and develop a liquid-metal-based hybrid sensor to study the qualitative and semiquantitative aspects of respiratory mechanics, monitoring the expansion and contraction of chest movements, exploiting the coupling of eutectic Ga–In alloy (EGaIn) and polydimethylsiloxane (PDMS), which show optimal characteristics to build a sensor for this application. The liquid metal has a suitable ohmic response and PDMS, due to its hyperelastic behavior and low viscosity, can be deformed easily and can transmit, without distortion, the primary frequency components useful to characterize different respiratory patterns, from slow and deep breathing to fast and shallow breathing. The time course and spectrum of the electric resistance signal from the sensor correspond closely to a standard reference obtained simultaneously by measuring chest deformation via optoelectronic stereophotogrammetry. The fabrication process is easy, cheap, and robust and can be industrialized.**

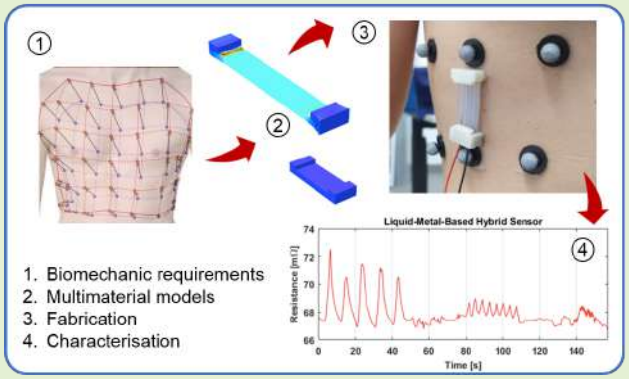

***Index Terms*— Biomechanical design, breathing monitoring, liquid metal, mechanical characterization, optoelectronic system, wearable sensor.**

I. Introduction

IN THE literature, there are several examples of applications of liquid metal and elastomer hybrid structures, used as sensing devices. The present work deals with the dimensioning of a similar device for wearable respiration sensing. Liquid metals, i.e., metals that are in the liquid state at room temperature, mostly belong to the alloys of Ga and In, sometimes combined with a ternary element, such as Sn. These alloys have attracted much attention because of their capacity to conduct electricity and heat, coupled with unique mechanical properties, which allow them to undergo extreme deformations, and self-heal. Their many possible applications range from microfluidics to soft robotics. They were found particularly interesting for the fabrication of wearable sensing devices, opening the possibility of using them in rehabilitation assessment, sports, or the monitoring and study of human body movements in general. The advantages of this kind of solution over other sensing methods lie in their lightweight, compactness, high deformability, low energy consumption, and low cost.

A. State of the Art

Several implementations of hybrid liquid-metal/elastomer systems can be found in the literature [1], [2], focusing on solutions optimized for sensing of the lower limb kinematics and hand or finger motions. In recent years, greater attention

Manuscript received 21 December 2022; accepted 9 January 2023. Date of publication 26 January 2023; date of current version 14 March 2023. The associate editor coordinating the review of this article and approving it for publication was Dr. Edward Sazonov. *(Corresponding author: Simone Pittaccio.)*

This work involved human subjects or animals in its research. Approval of all ethical and experimental procedures and protocols was granted by the Ethical Committee of the National Research Council of Italy (CNR) under Protocol No. 0065527/2019, and performed in line with the Declaration of Helsinki.

Fabio Lazzari and Jacopo Romanò are with the Institute of Condensed Matter Chemistry and Technologies for Energy (CNR-ICMATE), National Research Council of Italy, 23900 Lecco, Italy, and also with the Department of Chemistry and Materials Engineering (DCMIC), Politecnico di Milano, 20133 Milan, Italy.

Marco Gaviati, Lorenzo Garavaglia, and Simone Pittaccio are with the Institute of Condensed Matter Chemistry and Technologies for Energy (CNR-ICMATE), National Research Council of Italy, 23900 Lecco, Italy (e-mail: simone.pittaccio@cnr.it).

Digital Object Identifier 10.1109/JSEN.2023.3238358

is being paid to wearable prototypes devised for respiration monitoring [3], [4], [5]. Chen et al. [5] focused on the reduction of the mechanical hysteresis of the sensor, in order to minimize measurement errors. They demonstrated that appropriately designed wavy channels can lead to the desired result and showed that the sensor they developed can also be used to monitor breathing.

Other recent examples of liquid-metal-based sensor for respiration monitoring include the work of Huang et al. [6], who developed a wireless sensor using SnS_2 nanosheets, and Zhang et al. [7], who obtained a self-powered magnetoelectric sensor, which uses an arch-shaped air gap, connected in series with an oxygen mask in order to monitor respiration in patients that rely on assisted ventilation.

While the literature offers several examples of advanced methodologies for the fabrication of liquid-metal-based sensors for respiration monitoring, there is a general lack of focus on the identification of biomechanical requirements for said devices, which are not directly integrated into the design process.

B. Objective of the Study

The motivation of the present study is to develop a sensor, which is able to provide a qualitative measurement of the breathing amplitude, during the execution of specific motor tasks carried out during a training session, the learning of a sport exercise in the gym, or during home-based activities. Of course, with COVID-19 infections still rife and likely to remain so in the next years, it is sensible to develop new technologies that help keep people's health conditions under control in an easy, comfortable, and cheap way, maybe even remotely.

All the studies mentioned in Section I-A have a technology-based approach, where the main focus is the investigation of the fabrication technique and the characterization of the prototype, which appears to be the most common format [8]. Conversely, we motivate the present study by focusing on the design steps, highlighting the importance of a preliminary study of the biomechanical context. We thus demonstrate a more comprehensive methodological approach, which starts from the assessment of biomechanical requirements for a possible application to monitor the breathing pattern and then proceeds with both analytical and numerical modeling to obtain a functional design of the sensor. We then continued with the fabrication of the sensor prototype, choosing to embed liquid-metal eutectic Ga–In alloy (EGaIn) within a polydimethylsiloxane (PDMS) elastomeric matrix, exploiting a low-cost and reproducible patterning strategy that can be easily replicated industrially, for greater sustainability, even in lower income countries. This present article includes an extensive section on the dimensioning and modeling of the device, taking the moves from biomechanical considerations. We provide a detailed description of material behavior and multimaterial interaction: for instance, the role of hyperelasticity versus elasticity has been considered, as well as a fully 3-D treatment of the electromechanical interaction of the elastomer matrix with the incompressible conductive fluid and matrix. Optoelectronic analysis is used both to aid in the identification of the biomechanical requirements of the device and to complete the characterization of the prototype. To the best of our knowledge, it is the first time that this technology is employed in this manner in the design and characterization of liquid-metal-based wearable sensors to monitor breathing.

Finally, we discuss the applicability of this technology to respiration monitoring in nonclinical everyday settings.

This article is organized as follows. In Section II, we describe the synthesis of the liquid metal and present its properties. We then propose a method to identify the biomechanical conditions and modeling strategies to support the design of the sensor. We then describe the fabrication and characterization methods. In Section III, we first show a comparison of predicted and measured mechanical and electrical properties for the device and subsequently display the functional performance as assessed in in vivo conditions. Section IV is centered on the value of including biomechanical information and thorough modeling while devising the concept and dimensioning this type of wearable multimaterial sensors. Finally, after discussing the sensor performance and the limitations of this study, we draw our conclusion.

II. Materials and Methods

A. Synthesis and Properties

Define that EGaIn was obtained by melting together 75.5% in weight of Ga and 24.5% of In in a glass vial under an Ar-rich atmosphere. The vial was kept in a water bath at 45 °C for 4 h to obtain complete melting of the two components and allow diffusional mixing between them. During the process, a final slight stir of the glass vial ensured a complete mixing and the formation of a homogeneous EGaIn alloy (mass density: 6.25 g/cm^3; melting point temperature: 15.5 °C).

The resistance of the alloy batch prepared was measured at 25 °C from a thin column of liquid metal contained in a glass cylinder 480 mm (length) by 0.9232 mm (mean radius) using Resistomat TYP2305 (Burster, Gernsbach (BW), DE) with two levels of test currents (10 and 100 mA). The estimated resistivity ($n = 3$ measurements per current level, repeated on the same material after a week) was $\rho = (2.8095 \pm 0.1545)\ 10^{-7}$ Ωm (mean ± std), compared to tabulated values for this material: 2.94118×10^{-7} Ωm [9]. The measurement was done in air, disregarding the effect of possible Ga oxide formation, as that effect will not be controlled during the sensor fabrication. PDMS rubber Rhodosil (Bluestar Silicones, Lyon Cedex, FR) was prepared by mixing in 1:1 ratio the two components (A and B as indicated on the datasheet) and letting it rest for 24 h to keep the polyaddition reaction going to completion before starting any test. Tensile tests on 5-mm (gauge length) 2×3 mm^2 (cross section) samples were conducted using DMA Q800 (TA Instruments, New Castle (DE), USA). The specimen was fixed to the DMA clamps with a reference length of 5 mm, which was set using an ad hoc template to make preload repeatable. Applying ramps to a maximum strain $\varepsilon_{max} = 100\%$ (stretch ratio $\lambda_{max} = 2$) with a strain rate of 500%/min, the material was subjected to 50 cycles for stabilization. Subsequently, the uniaxial characteristic was measured and employed to fit different hyperelastic models (Neo-Hookean, Mooney–Rivlin,

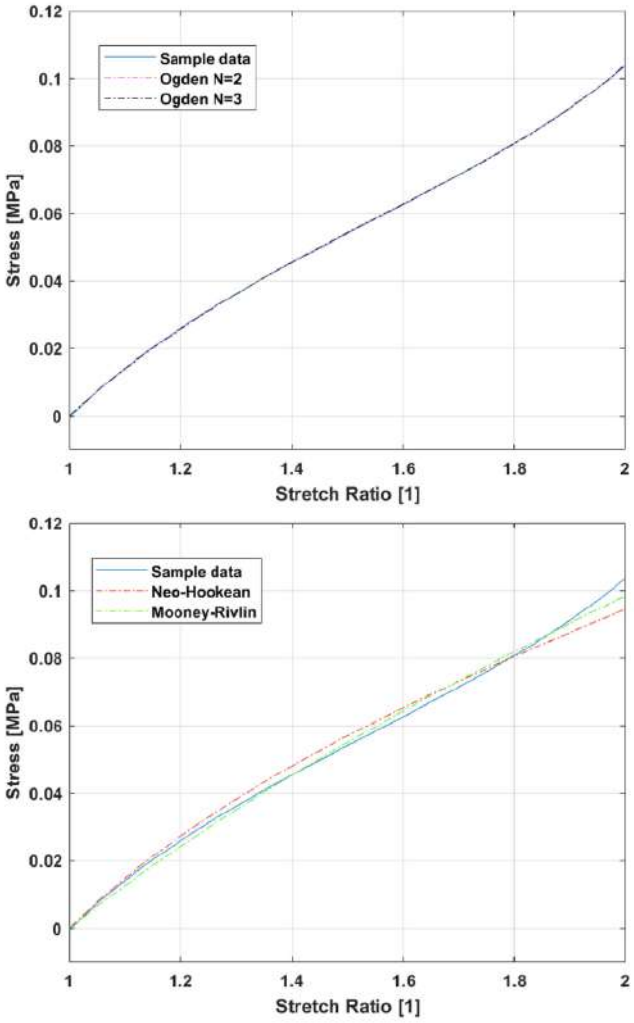

Fig. 1. Comparison of the best fits obtained on the PDMS uniaxial data for different hyperelastic models.

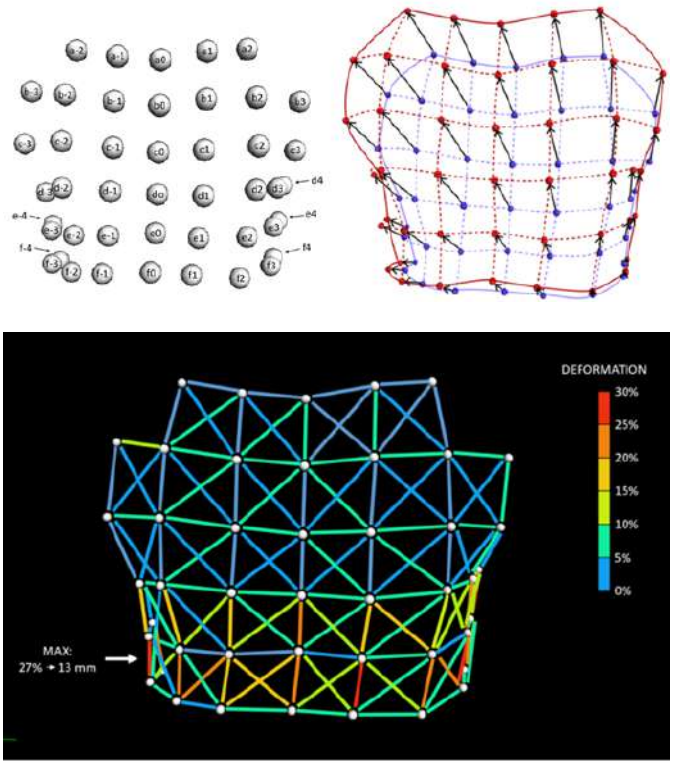

Fig. 2. (Top left) Markers names and positions on the anterior and lateral thorax: a0 is on the jugular process and the top row along the claviculae, all the other markers are positioned 5 cm away from their nearest neighbors. (Top right) 3-D thorax expansion due to breathing. In blue, marker positions in expiration, and in red, marker positions at maximum inspiration, the arrows showing the displacement vectors. (Bottom) Normalized difference between the minimum and maximum distances of all the horizontal, vertical, and diagonal pairs of neighbor markers. The maximum stroke is revealed for the vertical pair [e-3, f-3], lying on the right lower side of the rib cage.

Ogden N = 2, and Ogden N = 3 – Fig. 1). The Neo-Hookean fit ($\alpha = 2$ $\mu = 0.05395473$), albeit less accurate overall, is computationally more manageable. It represents the material behavior reasonably up to $\lambda = 1.6$.

B. Identification of the Biomechanical Conditions

The device to be designed will be used to sense basic respiration parameters (frequency and qualitative depth); consequently, some biomechanical constraints apply. The best location on the thorax and the corresponding expected elongation during respiratory actions was estimated using stereophotogrammetric measurements of thorax surface displacement (Vicon, Centennial, CO, USA, optoelectronic system equipped with 6 Vero 2.0 infrared cameras, controlled by the Nexus software). We have used a grid of 45 markers homogeneously spaced 5 cm from each other starting from a central column (from a0 to f0) that marks the sternum, as shown in Fig. 2. Local deformation of the ribcage surface was obtained by calculating the differences between the inter-marker (first and second nearest neighbors) Euclidean distances in extreme inspiration and expiration configurations, and dividing each by the corresponding expiration distance. The maximum estimated deformation was found to be 27% (a distance difference of 13 mm), the vertical pair [e-3, f-3], lying on the right lower side of the ribcage.

C. Design and Modeling

The design was approached by analytical and numerical methods. Analytically, we imagined the basic sensor as a cylindrical tube and employed incompressible hyperelastic assumptions for the PDMS wall [10] and pure incompressibility for the liquid metal inside the meatus. This method leads to the following expression for the electric resistance gain:

$$G_R(\lambda) = \frac{R_0 + \Delta R}{R_0} = 1 + \frac{\Delta L}{L_0}\frac{\pi r_0^2}{\pi (\Delta r)^2} = \frac{\lambda_z}{\left(\lambda_z^{-1/2}\right)^2} = \lambda_z^2 \tag{1}$$

where R_0 is the initial resistance; ΔR is the resistance change due to deformation; L_0 and r_0 are the initial length and radius of the tube meatus, respectively, and ΔL and Δr are their respective changes; and λ_z is the longitudinal stretch ratio. It results that G_R is not dependent on the starting geometry

of the system or on the material characteristics: it only depends on the stretch to which the tube is subjected.

Now, using an incompressible (Poisson's ratio $\nu = 0.5$) Neo-Hookean constitutive law for the PDMS wall, the analytically predicted axial stress is

$$\sigma_z(\lambda) = \mu\lambda_z^2 - p = \mu\left(\lambda_z^2 - \lambda_z^{-1}\right) \tag{2}$$

where p is the hydrostatic pressure and μ is the shear modulus in the Neo-Hookean model. Correspondingly, the force to be applied axially to obtain the required gain is

$$F_z(\lambda) = \mu\left(\lambda_z^2 - \lambda_z^{-1}\right)\left(B^2 - A^2\right) \tag{3}$$

where A and B are the inner and outer diameters of the tube, respectively. Considering these preliminary observations, the biomechanical constraints, and some additional practical requirements linked to the device fabrication and the signal acquisition, the basic dimensioning could be set as follows. We expect that the available forces exchanged with the ribcage to be in the range of few newtons.

Furthermore, we require the basic electric resistance of the liquid-metal pattern to be high enough (tens of milliohms), in order to guarantee a sufficient signal-to-noise ratio of the sensor, even with limited test currents (e.g., 100 mA). With a tube-like sensor of 30 mm in length (which would be compact and easy to handle), choosing an inner radius of the channel of 0.5 mm and an outer radius of 2 mm (easy to fabricate), we would expect an undeformed resistance of 11 mΩ and a required external force of 1.1 N to extend the sensor to 100% strain (i.e., a stretch ratio of 2). The resistance gain for 100% strain would be 4, and for an extension of 13 mm (see the biomechanical conditions), it would be slightly over 2. In order to increase the resistance without making the device longer, multiple tubes could be connected electrically in series and mechanically in parallel. Hence, we settled for a design like in Fig. 3(a). The entire sensor is 42 mm long and 14 mm wide. The central part, in which the metal-filled channels lie, is 3.5 mm thick, while the ends are 6 mm thick to facilitate the handling and make them less prone to deform under load. The inner channel has a square section of 0.9 mm side (equivalent to a circular section of 0.5 mm internal radius. The transverse connections between the four channel branches in the serpentine are kept short to minimize the unwanted effect of localized cross section distortions. A 3-D finite-element model (FEM) of the sensor was developed under Comsol Multiphysics 5.5 (COMSOL Inc.) to check the design.

The constitutive law for the silicone matrix was Neo-Hookean. The fluid was modeled as a very low-stiffness incompressible solid (Young's modulus $E = 100$ Pa), and hence, fluid dynamics was not considered. The other electromechanical material parameters were expressed in the previous sections. One extremity was fixed longitudinally, while an incremental displacement along the longitudinal direction was applied on the opposite end, up to a final stretch $\lambda_z = 2$. A constant current of 1 mA was injected at one end of the metal channel, while the other end of the metal is set to an electric ground. The computational mesh contained 12 990 tetrahedral elements. The solutions for the structural and electric problems were calculated using a segregated algorithm.

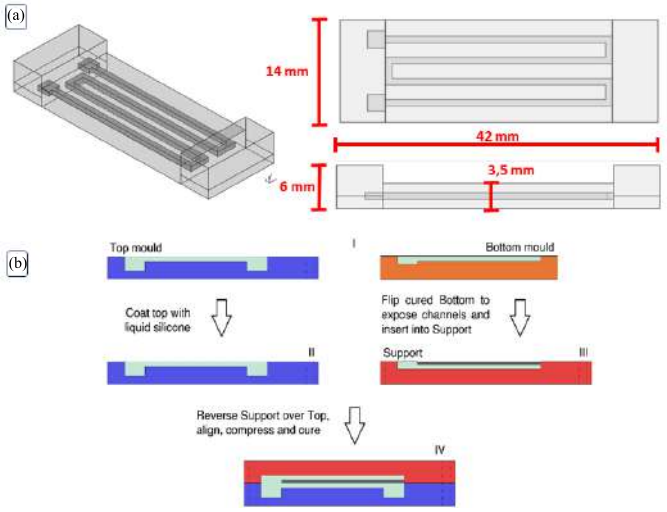

Fig. 3. Overall design of the sensor. (a) Axonometric, top and side view. (b) Representation of the adhesion process of the two PDMS parts (in light green). (I) In the top and bottom molds is poured 1:1 PDMS and left to complete cross-linking—microchannel negatives are highlighted in orange in the bottom part. (II) 2:1 liquid PDMS is spin coated on the flat part of the top mold. (III) Solid bottom part is turned upside down and moved into the support, with the microchannels exposed (highlighted in gray). (IV) Two molds are aligned and compacted with the bottom part above to prevent occlusion of the microchannels (highlighted in gray).

D. Fabrication and Assembling of the Sensor

The PDMS matrix was obtained by a multistep molding process similar to the one disclosed in [11] and [12]. In particular, two solid PDMS layers (top and bottom) are first obtained and later assembled through the application of a thin interlayer of uncured PDMS, which will join them upon curing. The top layer is smooth on one side and is characterized by thicker ends on the other. The bottom layer is made to contain the channels that will hold the liquid metal. The molding and assembling procedure are presented schematically in Fig. 3(b). The mold parts (top, bottom, and support) were 3-D printed with a Raise3D N2 Plus (Raise3D, Costa Mesa (CA), USA) using polylactic acid (PLA) filament. The extrusion nozzle was 0.4 mm in diameter. The layer thickness was set to 0.1 mm. The deposition of the uncured PDMS interlayer was done by spin coating about 0.3 g of liquid at 600 r/min for 120 s. While the two components of Rhodosil PDMS were mixed in the suggested 1:1 ratio for the solid layers, a 2:1 ratio in favor of component A was used for the interlayer, to help adhesion. After curing, the inner channels were filled with liquid-metal EGaIn using a syringe. The EGaIn alloy was freshly made just before the filling process so that the surface oxide film was very thin. The syringe was filled extracting the liquid metal from underneath the oxide film. Inserting the syringe in one of the two channel ends and leaving the other clear and open, the filling process was swift and smooth [see Fig. 4(a)]. As soon as the channel was filled up, including the two small reservoirs at the ends, the two electric wires were inserted,

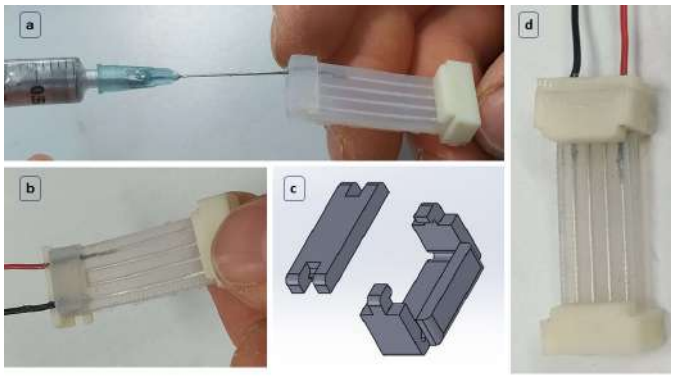

Fig. 4. Final assembling of the sensor. (a) With the use of a syringe, the freshly made EGaIn alloy is inserted into the channel of the PDMS device. (b) Electric connection is obtained by inserting the wires with the unsheathed end into the channels until the reservoir. (c) Three-dimensional printed snap-fit clamps are used to ensure mechanical stability to the electrical connections, seal the channels, and provide an interface with the skin. (d) Final version of the device ready to be used.

with unsheathed ends, until the reservoirs [see Fig. 4(b)]. This ensured a continuous electrical connection between the wires and the liquid metal. The final step was the application of 3-D-printed snap-fit clamps over the PDMS device extremities; those elements [see Fig. 4(c)] ensured the mechanical stability of the electrical connections and sealed the channel ends by compression. They were also convenient parts to apply some double-sided biomedical tape and attach the device to the skin.

E. Sensor Characterization

The technical tests on the sensor were carried out by combining (dynamic) mechanical and electric characterization. To this end, we used Instron ElectroPuls E3000 (Instron, Norwood, MA, USA) to produce the controlled deformation. Since the force full scale of this instrument is 5 kN, which was deemed too high for the present application, force was measured using an additional load cell Burster 8435 (Burster, Gernsbach (BW), DE), with a maximum load of 200 N, equipped with amplifier module 9243 (Burster, Gernsbach (BW), Germany) and powered at 24 V by Aim-TTi CPX400DP (Aim-TTi, Huntingdon (Cambs.), U.K.) power source. We have used Keithley 6220 (Keithley Instruments, Cleveland, OH, USA) as a stable source of current to inject 100 mA into the liquid-metal serpentine. Both the Burster load cell signal and the voltage from the serpentine have been acquired using a Eurotherm Nanodac (Schneider Electric, Rueil-Malmaison (IDF), France) that allowed us to synchronize the signals of force and resistance in phase during the tests. With this setup, the sensor was subjected to a minimum prestrain of 10% and controlled additional strain up to 70% at different frequencies (0.1, 0.5, 1, and 2 Hz) with a sinusoidal law. The sensor was then subjected to a low-strain-rate cycle to 100% in order to verify the resistance gain values obtained from the FEM simulations. Tests were conducted at 30 °C, to simulate the temperature conditions in proximity of the human body.

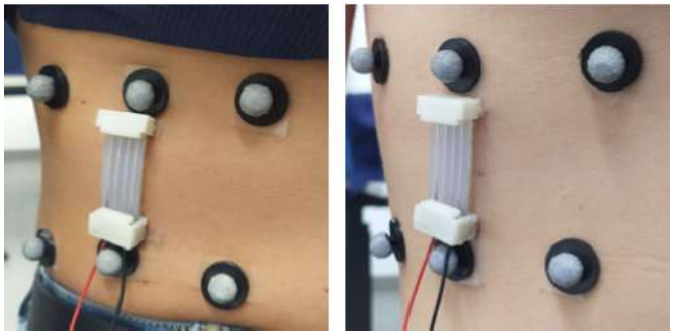

Fig. 5. Sensor was attached to the chest skin at the location of maximum expected stretch during a respiration cycle. Connections are to the electric current generator and the data logger. Reflective markers for optoelectronic stereophotogrammetry are placed on a fiducial grid (see Fig. 2). Photographs: mountings for S5 (left) and S7 (right).

F. Respiration Monitoring Test

The respiration monitoring ability of the sensor was tested by attaching the device to the chest and acquiring the voltage changes with various respiration patterns. The device was connected with a current generator Keithley 6220 (Keithley Instruments, Cleveland, OH, USA) and a data logger Eurotherm Nanodac (Schneider Electric, Rueil-Malmaison (IDF), France). For all the measurements, a current of 100 mA was injected in the liquid-metal coil. The sensor was placed on the position displaying, as verified, the maximum stroke during breathing, i.e., between e-3 and f-3 (see Fig. 2). Markers were placed on e-2, e-3, and e-4, and f-2, f-3, and f-4, and the sensor was placed in the middle of this 2 × 3 matrix. The optoelectronic system was used to acquire an external measurement of respiration. The sensor was fixed to the thorax skin using a double-sided adhesive tape (see Fig. 5). In doing so, a prestrain of approximately 15%–20% was imposed on the sensor, in order to ensure the sensor remained taut during all the measurements. With this setup, one healthy volunteer (25 years old, male) was asked to simulate different types of breathing: deep breathing with a complete expansion and contraction of the chest, normal breathing, and shallow breathing with fast breathing cycles of little amplitude. The healthy volunteer signed informed consent to the study. The method complies with the Declaration of Helsinki and received the approval of the Ethical Committee of the CNR (National Research Council of Italy), protocol number 0065527/2019. Both the optoelectronic and the sensor response were collected at the same time to have a comparison between the two systems and verify the correct functioning of the piezoresistive liquid-metal-based device. The optoelectronic distance between the e-3 and f-3 markers has been calculated, for every moment, as the difference between the vertical coordinates of the two markers. As the optoelectronic system acquires data at 100 Hz while the Eurotherm at a frequency of 8 Hz, the 100 Hz signal was downsampled to 8 Hz, before attempting any comparison. In addition to analyzing the measurements in the time domain, the signal spectral properties were also studied. The frequency spectra were obtained by exploiting the Welch method with a single Hamming window.

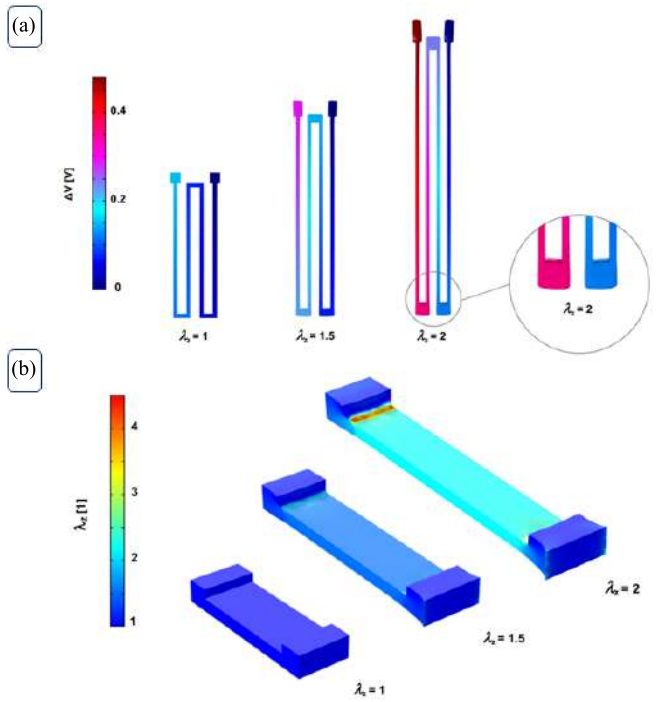

Fig. 6. (a) Numerical simulation of the deformation of the sensor along the *z*-axis. The sensor is constrained on the bottom-right end face and pulled at the other end to incremental stretches up to 100% strain ($\lambda_Z = 2$). (b) Corresponding deformation of the microchannels and voltages (color scale) for a constant current of 100 mA.

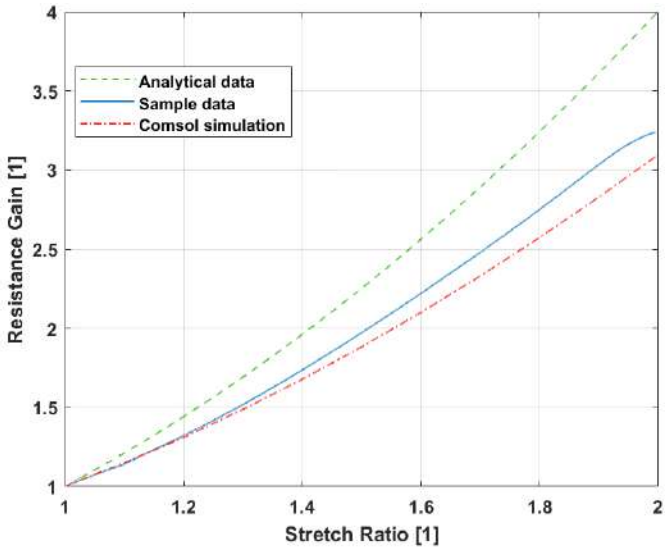

Fig. 7. Resistance gain versus stretch ratio of the sensor. The figure shows a comparison between the solutions of the simplified analytical model and the finite-element (*Comsol*) simulation. Both predictions are plotted against the experimentally obtained characteristic (*Sample*) of the multimaterial sensor.

The same procedures were then applied to test the device on additional seven subjects (33.0 ± 5.3 years old, two female), enrolled to verify repeatability with different anatomic features and breathing habits in the execution of a standard breathing pattern (three deep, three normal, and a few shallow breaths). The correlation between the optoelectronic (marker distance) and sensor-based (electric resistance) time courses was studied by computing the linear regression between the corresponding

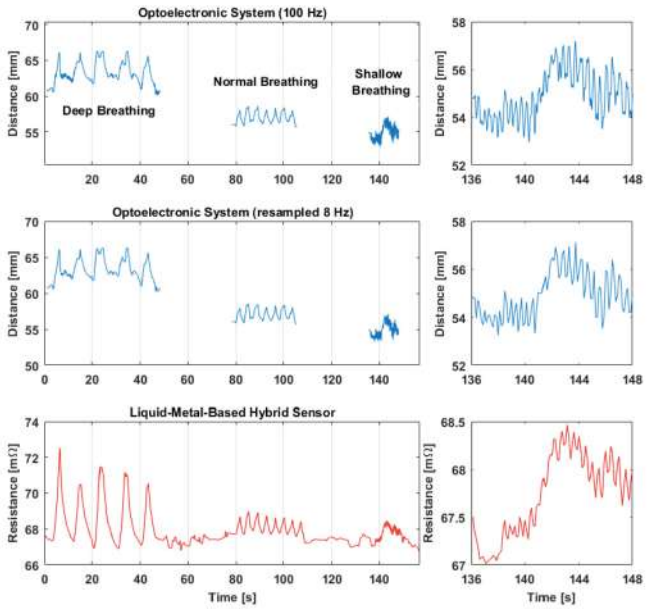

Fig. 8. Respiration monitoring by the optoelectronic system marker distance (*top*: original sampling and *middle*: downsampled) and simultaneously by the multimaterial sensor (electric resistance—*bottom*) for different types of breathing. The graphs on the *right* are magnifications of the shallow breathing section highlighting the similarities between the signal patterns.

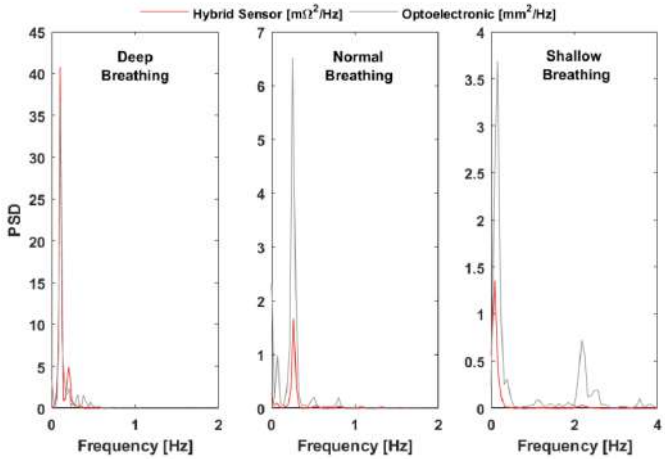

Fig. 9. Analysis of the frequency response of the sensor: PSD calculated for deep breathing (*left*), normal breathing (*middle*), and shallow breathing (*right*). The red graphs are referred to the measurements via the multimaterial sensor, while the gray graphs refer to the optoelectronic acquisition.

time points in the respective tracings. The fitting was obtained with the lowest degree polynomial that would provide a good fit (3°). The coefficient of determination R^2 was calculated for each subject, and then, we worked out the mean and standard deviations of R^2.

III. Results

A. Comparison of Computational and Experimental Properties

Fig. 6 shows the results of the FEM simulations of the sensor deformation. In Fig. 6(a), the principal axial stretch ratio field is plotted in false colors superimposed on the

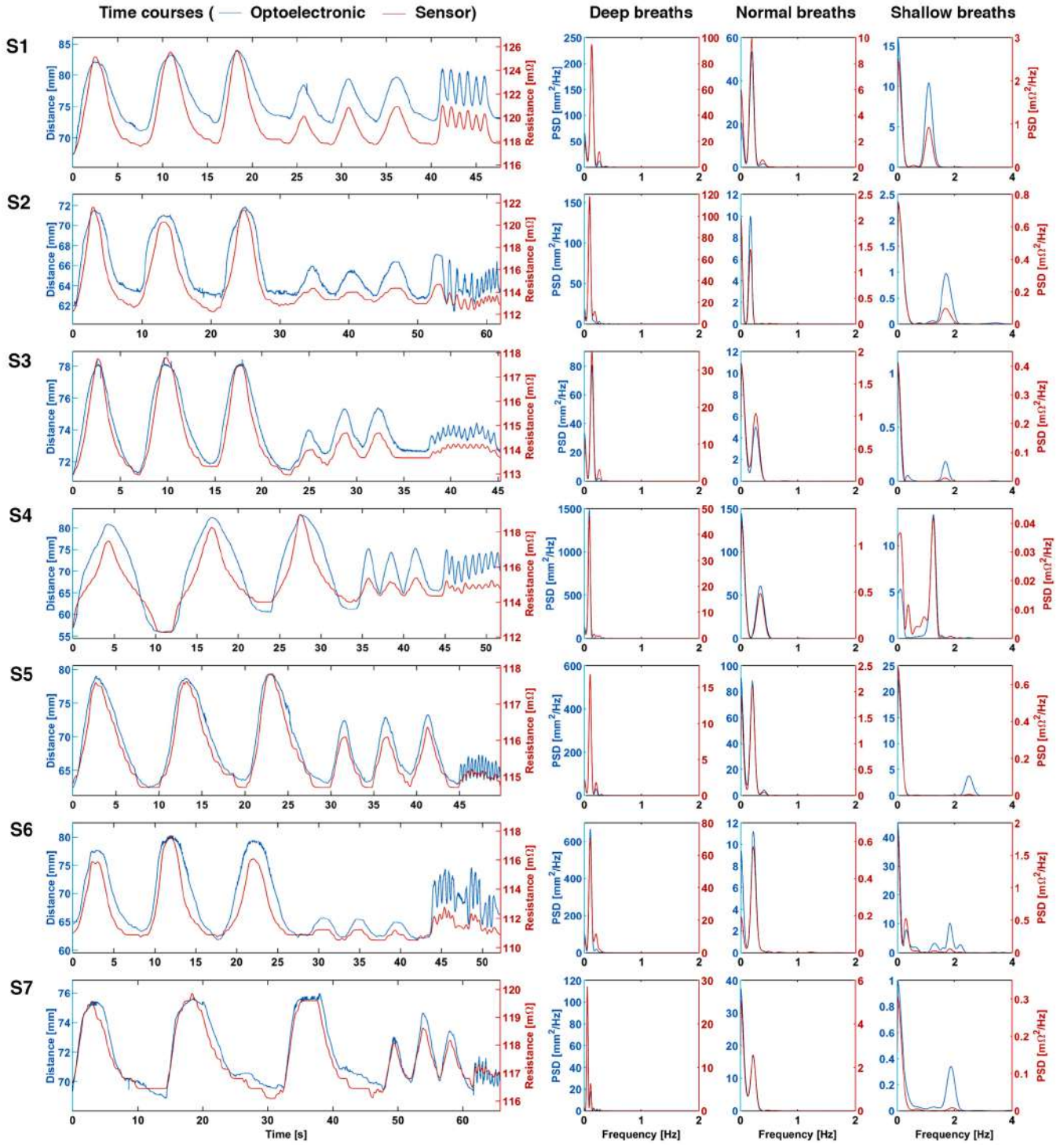

Fig. 10. Comparisons of the time courses (left) and power spectral densities (three plots on the right) of the reflective marker distances and corresponding sensor electric resistances for the seven additional subjects (S1–S7) enrolled for the device performance assessment.

deformed geometry for different applied external stretches. The presence of an increased cross section at the two ends of the sensor appears to be effective in minimizing strain concentration. The stretches are fairly homogeneous in the central region, allowing a quasi-uniform deformation in the liquid-metal serpentine [see Fig. 6(b)]. As expected, the transversal connections of the metal serpentine deform in an opposite way to the main branches (i.e., becoming thicker and slightly shorter). The voltage gradient is continuous. Fig. 7 shows the comparisons between the analytical and numerical estimations of the functional relationships of resistance gain versus stretch ratio. The analytical estimate was obtained by observing that the sensor is roughly four tubes connected mechanically in parallel and electrically in series. This means that all branches of the serpentine stretch in the same way (uniform stretch in the series, equal to

one single branch) can be seen as a 4× longer current path (increasing the resistance) and cooperate by acting in parallel to raise by 4× the force needed to produce the stretch. The external force calculated numerically evolves similar to the analytical case, with lower predicted values. From Fig. 6, the difference can be attributed to inhomogeneities in the stretch field near the thickened ends and around the microchannel interconnections: the nonidealities should not invalidate the function of the sensor that deforms in a homogeneous way throughout its central thinner area, which contains the liquid-metal-filled microchannels. Indeed, the resistance gain though reaching values somewhat reduced with respect to the analytically based design undergoes a threefold increment between the undeformed ($\lambda_z = 1$) and fully stretched ($\lambda_z = 2$) conditions. In this case, the differences are probably due to the local deformation of the interconnections between the four branches of the serpentine: their contribution to the resistance gain is negative and should not be neglected. The trend obtained numerically for the resistance gain versus stretch ratio corresponds closely to the one calculated from the experimental measurement (see Fig. 7). The results of the (experimental) dynamic characterization showed that a transitory can be observed during the initial part of the test (0.1 Hz), affecting in particular the resistance signal, but also the force time course, which levels out in a matter of some seven cycles, after which the response reaches a repeatable behavior.

B. Results of Respiration Monitoring

A comparison between the electric resistance signal acquired through the liquid-metal-based hybrid sensor, worn on the chest during breathing, and the intermarker distance obtained from the optoelectronic system is reported in Fig. 8. The top of graph has reported the original signal from the optoelectronic system with a sampling frequency of 100 Hz, while the middle and bottom rows have been reported the optoelectronic data downsampled to 8 Hz and the multimaterial sensor measurement, respectively. The sensor follows very well the elongation of the body portion, to which it is attached. Deep breathing, producing marker displacements close to the maximum estimated stroke on the skin, generated very neat peaks in the sensor resistance signal. Normal breathing is also clearly appreciable, and each successive breathing cycle can be distinguished from the others. Also, shallow breathing can be revealed using the sensor, and its high frequency and limited amplitude are represented in the sensor resistance signal. Every breath is represented and countable, and even the baseline is similar. From these observations, it appears that the sensor resistance signal is qualitatively coherent with that obtained from the variable distance between the two markers chosen for the optoelectronic-based monitoring. Correspondingly, in the frequency domain (see Fig. 9), it can be appreciated that, although the absolute power spectral density (PSD) values between the optoelectronic and sensor signals are different, the overall pattern is remarkably similar. The principal frequency bands are captured by the sensor, and the power intensity ratios between the main

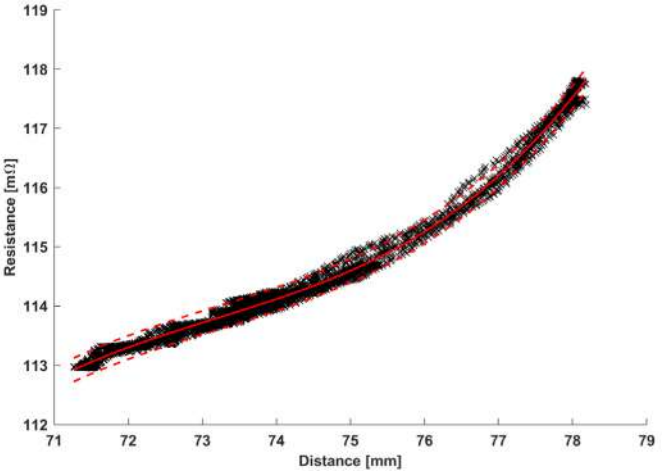

Fig. 11. Example of 3° polynomial regression between corresponding points (scatter plot) on the reflective marker distance and sensor electric resistance time courses. The solid and dashed curves show the polynomial fit and the confidence range of ± one standard error on the prediction. The coefficient of determination, in this case, is equal to $R^2 = 0.993$ (best result).

spectral components are compatible, if not alike, despite a tendency to underestimate higher frequency rhythms.

Similar observations can be made for the additional subjects, thus confirming the repeatability of the measurement characteristics. Fig. 10 shows the time courses and power spectra for the seven subjects, while Fig. 11 shows an example of the regression results. Collectively, it can be stated that the observed correlation between the optoelectronic measurement and the signal time course is very good ($R^2 = 0.977 \pm 0.014$, mean ± standard deviation, and $n = 7$).

IV. Discussion

This work addressed the exploitation of functional and hybrid materials in the field of wearable soft sensors, especially for the monitoring of breathing. The methods we employed are robust and encompass the basic characterization of materials, the definition of analytical and numerical models to study the combined behavior of liquid metal and PDMS, the design and fabrication of the device, and a demonstration of its application in relevant operation conditions. The pipeline we have adopted (see Fig. 12) can be suggested for the design of new sensing devices based on liquid metals and PDMS.

A. Biomechanical Information as a Useful Basis for Sensor Design

The preliminary assessment of the skin deformation and the location of the maximum deformation length during breathing was very helpful to select an initial dimensioning of the device and to predefine an optimal location for its final application. In order to optimize for specific purposes this type of sensor, whose general design has been developed by other groups for different uses, we find certainly advisable to gain sufficient quantitative description of the relevant biomechanical environment in order to size the channels and matrix correctly.

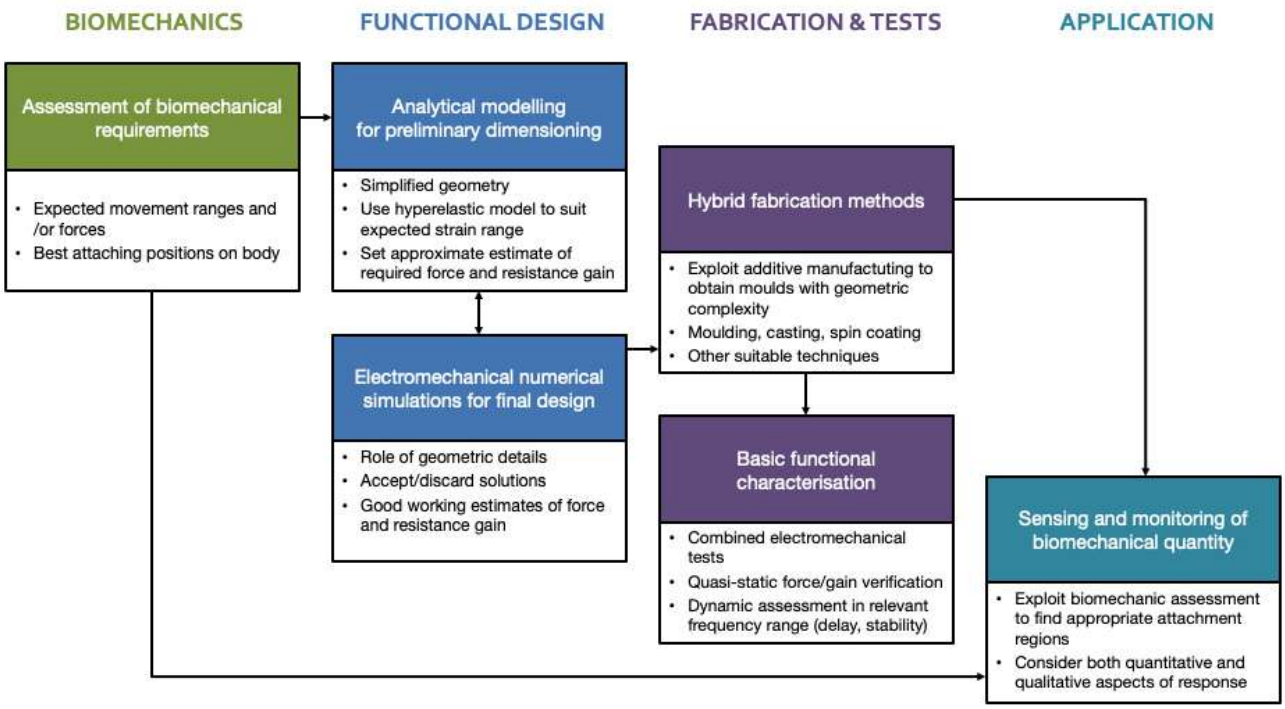

Fig. 12. Schematic of the pipeline adopted for the design of the hybrid material sensor in this study. The same approach can be suggested for the development of innovative biomechanical applications of this type of device.

B. Value of Different Methods for Multimaterial Interaction Modeling

For the sensor design process, we employed and compared ad hoc analytical and numerical methods for multimaterial and multiphysics modeling. The analytical treatment was helpful to gain insight into the fundamental relationships linking the mechanical and electrical responses of the multimaterial structure: in particular, it highlighted the strong connection between the stretch ratio and the resistance gain, independent of the matrix properties, and the effect of material hyperelasticity and incompressibility on the expected reaction forces. Comparing the simplified analytical scheme with the numerical results, it appears that in this case, the analytical method is appropriate for a first design drafting and dimensioning phase but may be unsuitable to predict precise external forces or resistance gains. Those are best captured by a 3-D FEM procedure. The numerical simulations were able to predict quite well the quantitative behavior measured experimentally in controlled conditions and were helpful to explain the relationships between local morphological characteristics of the design (i.e., thickened ends and channel interconnections) and functional nonidealities.

C. Sensor Performance and Possible Applications

The sensor characterization, carried out in controlled conditions with an ad hoc setup, has highlighted that its functionality is similar to that predicted by the FEM simulations. With the proposed design, the sensor was able to let the microchannels deform uniformly and produce a variation of the electrical signal with a difference of 22.5% with respect to the ideal (analytically estimated) gain at 100% strain, i.e., GR (2) = 3.15 versus 4. The forces necessary to deform the sensor are consistent with those computed during the design phase. The signal has good repeatability over tens of strain cycles up to 70%–100% of deformation with different frequencies, and the initial stabilization transitory is short (less than ten cycles), which is consistent with the low viscosity of PDMS. We developed a strongly application-related setup using optoelectronic stereophotogrammetry to acquire respiratory movements to compare with variations in the resistance signal from the sensor. Optoelectronic stereophotogrammetry has been used extensively to study breathing patterns and was taken here as a standard reference method [13]. In the respiration monitoring tests, the sensor demonstrated its versatility and precision: from its resistance signal, it is possible to distinguish visually and quantitatively several types of breathing patterns, which have different amplitudes and frequencies, and we have confirmed these capabilities using optoelectronic methods that allowed measuring the distance of the two points at the extremities of the sensor during time. The signals sensed by the hybrid material device and the optoelectronic system display very strong similarities in both the time and frequency domains. The effective resistance gain obtained with the present biomechanically optimized design proved high enough to sense very small ribcage deformations, in the range of a few tenths of millimeters with a 100-mA probe current. The sensing possibilities of the sensor suggest its usefulness in particular to monitor and evaluate the respiratory rate (RR), which is an important indicator of a person's health and fitness state [15], not only during athletic training [15] or the learning of a new motor task but also in daily life [16]. In some cases, its fluctuations from the normal range of values can

predict serious clinical events such as cardiopulmonary arrest or chronic heart failure [17]. Furthermore, these days more interest has emerged due to the spreading of the pandemic: in fact, irregular breathing can be related also to serious conditions due to the COVID-19 infection [18]. The RR could be estimated automatically by one of many existing peak identification algorithms in the time domain or by calculating the main principal frequency components [19]. Also, a qualitative measurement of the breathing amplitude could be attempted, especially in connection to the execution of home-based breathing tests, specific motor tasks carried out during a training session or during the learning of a sport exercise in a gym, rather than during free daily activities. These signal processing procedures remain to be detailed and tested in future.

D. Limitations of This Work and Future Perspectives

The sensor, as it was built and tested, is a prototype. Although its fabrication procedure was reproducible, some design details concerning the solidity of the liquid-metal/electric-cable connections could be improved, e.g., by ensuring a stabler contact between the cable sheath and the PDMS matrix holes. Furthermore, for real use as a wearable device, the sensor should be complemented with a current supply (battery-based) and an electronic unit able to manage the powering and to acquire and transmit the signal. Those remain to be chosen/designed. The effect of using different (smaller) test currents on the signal-to-noise ratio also needs to be addressed because this could extend battery life. Given the present quality of the signal, there are fair chances that lower currents could be employed.

V. Conclusion

In the light of precise biomechanical constraints and through the study of analytical and numerical models aimed to predict the behavior of multimaterial system EGaIn-PDMS, we have successfully developed a liquid-metal-based hybrid sensor applicable to the study of qualitative and semiquantitative aspects of respiratory mechanics, monitoring the expansion and contraction movements of the chest. EGaIn and PDMS showed optimal characteristics to build a sensor for this application: the liquid metal has a suitable ohmic response and PDMS, due to its hyperelastic behavior and low viscosity, can be deformed easily and is able to transmit, without distortion, the primary frequency components useful to characterize different respiratory patterns from slow and deep breathing to fast and shallow breathing. The time course and spectrum of the electric resistance signal from the sensor correspond closely to a standard reference obtained simultaneously by measuring chest deformation via optoelectronic stereophotogrammetry. The design of the sensor is very simple, but functional to its purpose, and barely complements the intrinsic properties of the hybrid material. The fabrication process is easy, cheap, and robust and could be industrialized, by further implementing a wearable supply and signal processing unit.

Acknowledgment

The study has been conducted in the laboratory of CNR–ICMATE at Lecco. The authors would like to thank Enrico Bassani from CNR–ICMATE for the technical support during the design and development of the prototype.

Statements and Declarations

Conflict of Interest: The authors certify that they have no affiliations with or involvement in any organization or entity with any financial interest, or nonfinancial interest in the subject matter or materials discussed in this article; furthermore, this article has not been previously published and is not being considered for publication elsewhere in whole or in part in any language.

Data Availability: The datasets generated during and/or analyzed during the current study are available from the corresponding author on reasonable request.

Consent to Participate: Informed consent was obtained from all individual participants included in the study.

Consent to Publish: All the subjects provided consent by signing an informative agreement about the purpose of the study and the treatment of the data collected.

Code Availability: The custom codes generated during the current study are available from the corresponding author on reasonable request.

Author Contributions: The authors have made substantial contributions to all the following: 1) the conception and design of the study, or acquisition of data, or analysis and interpretation of data; 2) drafting the article or revising it critically for important intellectual content; 3) final approval of the version to be submitted; and 4) furthermore, they agree to be accountable for all aspects of the work in ensuring that questions related to the accuracy or integrity of any part of the work are appropriately investigated and resolved.

References

[1] L. Liu, "Recent advances in printed liquid metals for wearable healthcare sensors: A review," *J. Phys. D, Appl. Phys.*, vol. 55, no. 28, Oct. 2022, Art. no. 283002.

[2] P. Won, S. Jeong, C. Majidi, and S. H. Ko, "Recent advances in liquid-metal-based wearable electronics and materials," *iScience*, vol. 24, no. 7, Jul. 2021, Art. no. 102698.

[3] J. H. Oh, J. Y. Woo, S. Jo, and C.-S. Han, "Pressure-conductive rubber sensor based on liquid-metal-PDMS composite," *Sens. Actuators A, Phys.*, vol. 299, Nov. 2019, Art. no. 111610.

[4] Y. Li, "A soft polydimethylsiloxane liquid metal interdigitated capacitor sensor and its integration in a flexible hybrid system for on-body respiratory sensing," *Materials*, vol. 12, no. 9, p. 1458, 2019.

[5] J. Chen et al., "Superelastic, sensitive, and low hysteresis flexible strain sensor based on wave-patterned liquid metal for human activity monitoring," *ACS Appl. Mater. Interfaces*, vol. 12, pp. 22200–22211, Apr. 2020.

[6] Y. Huang, F. Yang, S. Liu, R. Wang, J. Guo, and X. Ma, "Liquid metal-based epidermal flexible sensor for wireless breath monitoring and diagnosis enabled by highly sensitive SnS_2 nanosheets," *Research*, vol. 2021, pp. 1–13, Jan. 2021.

[7] X. Zhang, J. Ai, R. Zou, and B. Su, "Compressible and stretchable magnetoelectric sensors based on liquid metals for highly sensitive, self-powered respiratory monitoring," *ACS Appl. Mater. Interface*, vol. 13, no. 13, pp. 15727–15737, Apr. 2021.

[8] W. Zhang and R. Huang, "Liquid metal based flexible and implantable biosensors," *Biosensors*, vol. 10, no. 11, p. 170, 2020.

[9] T. Daeneke, "Liquid metals: Fundamentals and applications in chemistry," *Chem. Soc. Rev.*, vol. 47, no. 11, pp. 4073–4111, 2018.

[10] R. W. Ogden, *Non-Linear Elastic Deformations*. North Chelmsford, MA, USA: Courier Corporation, 1997.
[11] Y. Mengüç, "Soft wearable motion sensing suit for lower limb biomechanics measurements," in *Proc. IEEE Int. Conf. Robot. Automat.*, May 2013, pp. 5309–5316.
[12] Y. Mengüç, "Wearable soft sensing suit for human gait measurement," *Int. J. Robot. Res.*, vol. 33, no. 14, pp. 1748–1764, 2014.
[13] P. Laveneziana, "ERS statement on respiratory muscle testing at rest and during exercise," *Eur. Respiratory J.*, vol. 53, no. 6, pp. 1–34, 2019.
[14] W. D. Smyth, "Breathing pattern disorders distinguished from healthy breathing patterns using optoelectronic plethysmography," *Transl. Sports Med.*, vol. 2022, p. 11, Dec. 2022.
[15] C. M. E. Smyth, S. L. Winter, and J. W. Dickinson, "Optoelectronic plethysmography derived breathing parameters can differ between athletes with and without a dysfunctional breathing pattern during exercise," in *Proc. IEEE Int. Workshop Metrol. Ind. IoT*, Jun. 2020, pp. 54–58.
[16] B. Mendes, "Optoelectronic plethysmography: Reference values for breathing pattern," *Eur. Respiratory J.*, vol. 56, p. 2871, Jan. 2020.
[17] H. Liu, "Recent development of respiratory rate measurement technologies," *Physiolog. Meas.*, vol. 40, no. 7, 2019, Art. no. 07TR01.
[18] L. Purnomo and H. Adiprabowo, "Non-contact monitoring and classification of breathing pattern for the supervision of people infected by COVID-19," *Sensors*, vol. 21, no. 9, p. 3172, 2021.
[19] M. A. Motin, C. K. Karmakar, and M. Palaniswami, "Ensemble empirical mode decomposition with principal component analysis: A novel approach for extracting respiratory rate and heart rate from photoplethysmographic signal," *IEEE J. Biomed. Health Informat.*, vol. 22, no. 3, pp. 766–774, May 2018.

Fabio Lazzari was born in Lecco, Italy, in 1988. He received the B.S. and M.S. degrees in electronic engineering in 2010 and 2015, respectively. He is now completing the Ph.D. degree in Materials Engineering with the Politecnico di Milano, Milan, Italy.

Since 2015, he has been working at the National Research Council of Italy, Institute of Condensed Matter Chemistry and Technologies for Energy (CNR-ICMATE), Lecco, Italy. His research interests include sensors and wearable devices, the development and optimization of shape memory alloy-based soft robots, and the design of robotic devices for neuromotor rehabilitation.

Marco Gaviati was born in Carate Brianza, Milan, Italy, in 1996. He received the B.S. and M.S. degrees in Materials Science from the University of Milan-Bicocca, Milan, in 2019 and 2021, respectively.

He worked on his master's thesis during an internship at CNR-ICMATE, Lecco, Italy, on elastomer-metal hybrid materials for sensor applications. Since 2021, he has been with STMicroelectronics, Agrate, Milan, as a Lithography Process Engineer.

Lorenzo Garavaglia was born in Milan, Italy, in 1985. He received the B.S., M.S., and Ph.D. degrees in biomedical engineering from the Politecnico di Milano, Milan, in 2007, 2009, and 2017, respectively.

Since 2010, he has been working at the National Research Council of Italy, Institute of Condensed Matter Chemistry and Technologies for Energy (CNR-ICMATE), Lecco, Italy. His research interests include design and applications of shape memory alloys in neurorehabilitation and Sports Science where the evolution of wearable sensors found application in the monitoring of motor activity in order to improve sports performance.

Jacopo Romanò was born in Milan, Italy, in 1992. He received the B.S. and M.S. degrees in Biomedical Engineering in 2014 and 2016, respectively. He is now completing the Ph.D. degree in Materials Engineering with the Politecnico di Milano, Milan, Italy.

Since 2017, he has been working at the National Research Council of Italy, Institute of Condensed Matter Chemistry and Technologies for Energy (CNR-ICMATE), Lecco, Italy. His research interests include virtual design and smart materials applied to wearable devices and sensors for rehabilitation and healthcare.

Simone Pittaccio was born in Milan, Italy, in 1975. He received the B.A. degree in mandarin language and culture from IsIAO, Milan, in 1996, the Laurea degree in Biomedical Engineering from Politecnico di Milano, Milan, in 2001, and the Ph.D. degree from the University College London, London University, London, U.K., in 2004.

Since 2004, he has been with the National Research Council of Italy, Lecco, Italy, first as a Research Fellow and currently as a Researcher. He is also an Adjunct Professor of Metals Science and Sustainability at the Università degli Studi di Milano–Bicocca, Milan. His research interests include application of functional materials in the design of advanced technologies for neuromuscular rehabilitation and sports.

Mr. Pittaccio is a Founding Member of the Italian Bioengineering Group and a member of the Metals and Applied Technology Centre of the Italian Association of Metallurgy.

Open Access funding provided by 'Consiglio Nazionale delle Ricerche-CARI-CARE' within the CRUI CARE Agreement